Materials Today Bio 24 (2024) 100912

Contents lists available at ScienceDirect

Materials Today Bio

journal homepage: www.journals.elsevier.com/materials-today-bio

Cobalt-doped layered hydroxide coating on titanium implants promotes vascularization and osteogenesis for accelerated fracture healing

Xiaodong Chen [a,1], Shuohan He [a,1], Yilong Dong [b,1], Maohua Chen [a], Zengzilu Xia [a,***], Kaiyong Cai [a,**], Yan Hu [a,*]

[a] College of Bioengineering, Chongqing University, Chongqing 400044, China
[b] Department of Orthopaedics, The Third Affiliated Hospital of Wenzhou Medical University (Ruian People's Hospital), Wenzhou 325016, China

ARTICLE INFO

Keywords:
Bone defect repair
Layered hydroxide coating
Ti implants
Angiogenesis
Osseointegration

ABSTRACT

Angiogenesis at the fracture site plays crucial roles in the endogenous osteogenesis process and is a prerequisite for the efficient repair of implant fixed bone defects. To improve the peri-implant vascularization of titanium implant for accelerating defect healing, we developed a Co-doped Mg–Al layered hydroxide coating on the surface of titanium using hydrothermal reaction and then modified the surface with gallic acid (Ti-LDH/GA). Gallic acid coating enabled the sustained release of Co^{2+} and Mg^{2+} to the defect site over a month. Ti-LDH/GA treatment profoundly stimulated the angiogenic potential of endothelial cells by upregulating the vascularization regulators such as vascular endothelial growth factor VEGF) and hypoxia-inducible factor-1α (HIF-1α), leading to enhanced osteogenic capability of mesenchymal stem cells (MSCs). These pro-bone healing benefits were attributed to the synergistic effects of Co ions and Mg ions in promoting angiogenesis and new bone formation. These insights collectively suggested the potent pro-osteogenic effect of Ti-LDH/GA through leveraging peri-implant vascularization, offering a new approach for developing biofunctional titanium implants.

1. Introduction

Titanium (Ti) and its alloys are extensively utilized as orthopedic implants owing to their exceptional mechanical and biological characteristics. However, the biological inertness of titanium-based implants severely impedes new bone formation at peri-implant region, leading to suboptimal osseointegration and elevated risk of implant failure [1–4]. To overcome this limitation, several surface modification methods have been developed, including hydrothermal treatment, micro-arc oxidation, plasma injection, apatite coating, and organic polymer coating [5–9]. Among these techniques, hydrothermal treatment is a widely employed approach for *in situ* production of biofunctional coatings with intricate micro- and nano-morphology. For instance, Bai et al. reported the hydrothermal reaction-assisted formation of bionic coating on titanium surfaces that could promote osseointegration [10]. Shen et al. also effectively established coatings composed of micro- and nano-metal-organic framework (MOFs) on titanium-based surfaces via hydrothermal reaction, which demonstrated promising anti-inflammatory properties and antibacterial effects to improve new bone formation in the context of infected bone defects [11]. Meanwhile, layered double hydroxides (LDHs) are a type of ionic compound, consisting of stacked positively charged layers separated by interlayer anions and water molecules. LDHs are an emerging class of inorganic biomaterials with high biocompatibility and unique functions, which have garnered significant interest for *in vivo* application [12]. The functional versatility offers tremendous opportunities for various biomedical applications such as drug delivery and bone tissue engineering [13,14]. Interestingly, owing to their hydrolysis capacity, LDH could modulate the pH conditions of the tissue microenvironment upon implantation by scavenging environmental protons to eliminate excessive acidity [15]. This trait can substantially stimulate the proliferation of osteoblasts and promote osteoblastic differentiation, which provides unique advantages over other surface engineering methods for modulating bone microenvironment for accelerating bone regeneration and

* Corresponding author.
** Corresponding author.
*** Corresponding author.
E-mail addresses: zzlxia@cqu.edu.cn (Z. Xia), kaiyong_cai@cqu.edu.cn (K. Cai), huyan303@cqu.edu.cn (Y. Hu).
[1] These authors contributed equally to this work.

https://doi.org/10.1016/j.mtbio.2023.100912
Received 25 August 2023; Received in revised form 28 November 2023; Accepted 10 December 2023
Available online 21 December 2023

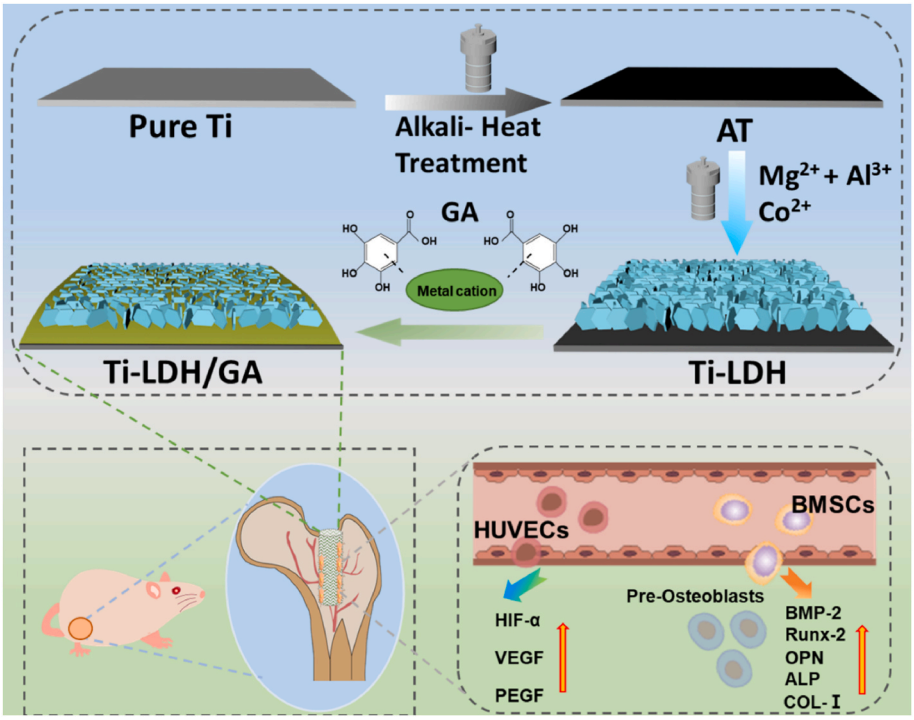

Fig. 1. Schematic illustration of the study. GA coating acts as gatekeepers to potentiate continuously release of Mg and Co ions from the underlying LDH layer at steady rates, thus maximizing their pro-osteogenesis efficacy through promoting local angiogenesis while avoiding acute toxicity.

enhancing bone repair [16–19]. For instance, Li utilized Mg–Fe bilayer hydroxide on the surface of a titanium implant to facilitate osteogenesis [20]. Chen prepared Sr, Ga LDH on the titanium implant surface through a hydrothermal reaction to improve osseointegration [21]. These studies highlighted the potential utility of LDHs for Ti implant modification.

There is abundant evidence that bone tissues rely on their vascular system to maintain bone homeostasis, which has profound impact on the osteogenic activity of osteocytes [22,23]. Neovascularization is particularly important during primary skeletal development and fracture repair, which is widely recognized as a crucial prerequisite for bone formation [24–26]. The distribution of blood vessels changes dynamically with bone growth and plastic transformation [27–29]. Early local vascularization following bone grafting provides a range of crucial nutrients for osteogenic activity and also plays a critical role in connecting bone to adjacent tissues and organs [30,31]. Consequently, vascularization at bone defect sites has emerged as a promising target to improve implant osseointegration and bone repair. Interestingly, multiple metal ions have demonstrated pro-angiogenesis capacities with no obvious side effects [32–35]. For instance, Jin-Woo et al. utilized Ca and Mg ions to dope the surface of titanium implants and discovered that Mg-doped implants had a greater effect on the early osteogenic differentiation of MSCs [36] Yu employed plasma injection to introduce Mg and Zn ions onto the surface of titanium implants, which displayed superior pro-osseointegration abilities through promoting local angiogenesis and osteoblastic differentiation, accompanied with enhanced binding strength at the bone-implant interface [37]. Additionally, previous studies have demonstrated that Co^{2+} can stimulate angiogenesis by creating a hypoxic environment to stimulate HIF signaling [38–40]. Fan utilized cobalt chloride to treat bone marrow stromal cells and observed that it could promote vascularized bone formation *in vivo* [41]. Huang utilized cobalt-loaded electrospun wire implants to enhance vasculature regeneration in diabetic rats [42]. Wu incorporated cobalt ions into bioactive glass and collagen aminoglycan scaffolds to develop a scaffold with both angiogenic and osteogenic capabilities [43]. LDH-based coating provides a facile approach for introducing metal ion-releasing depots on titanium surface, but long-term stable ion release from LDH remains a challenging task, which is essential for improving the therapeutic efficacy and safety of the biofunctional implants [44,45]. Recent studies showed that the abundant phenol groups in naturally occurring polyphenols can stably bond with alkalic metal ions and further regulated their release kinetics from the chelated substrates [46]. Gallic acid (GA) is a plant-derived biocompatible polyphenol with antioxidant, anti-inflammatory and pro-osteogenic activities [47]. However, the rational implementation of GA for modifying the metal ion release profiles from biofunctional implant surfaces is still rare despite its multifaceted therapeutic promises. Based on the scientific and technological insights described above, herein, Ti-LDH/GA was produced through the in-situ growth of Co-doped Mg–Al bilayer hydroxide (LDH) containing Co ions on the Ti substrate with a GA coating on its surface by hydrothermal reaction. Upon implantation *in vivo*, GA coating could facilitate the adhesion of bone healing-related cells on the implant surface while enabling controlled and sustained release of Mg^{2+} and Co^{2+}, which could synergistically promote angiogenesis at the bone defect site to accelerate the production of new bone at the bone-implant interface, eventually leading to robust osseointegration and defect healing (Fig. 1). The findings of this study could provide an approach to improve the performance of titanium orthopedic implants in the clinics.

2. Materials and methods

2.1. Materials

Pure Ti flakes and Ti rods were purchased from Fuxin Co. Ltd, China. Magnesium nitrate ($Mg(NO_3)_2$–$6H_2O$, 99 %) was purchased from J&K Chemical, China, aluminum nitrate ($Al(NO_3)_3 \cdot 9H_2O$), cobalt nitrate ($Co(NO_3)_2 \cdot 6H_2O$, 99 %) were purchased from Macklin, China. Gallic acid, CCK-8 assay kit and 4 % paraformaldehyde solution were purchased from Solaibao. Alizarin red (RAS) was purchased from Sigma, USA. Bicinchoninic acid (BCA) kit, 5-bromo-4-chloro-3-indolyl phosphate *P*-toluidine salt/Nitrotetrazolium Blue chloride (BCIP/NBT) staining kit and alkaline phosphatase assay (ALP) kit were purchased from Beyoncé, China. Rhodamine-ghost pencil ring peptide was purchased from

Thermo Fisher Scientific, USA. Total RNA extraction kit was purchased from Omega, USA. RNA reverse transcription kit and Real-time PCR (qPCR) quantitative assay kit were purchased from Takara, Japan.

2.2. Preparation of Ti-LDH/GA

Titanium foils were first ultrasonically cleaned twice with ethanol and deionized water for 30 min and 15 min, respectively, followed by drying in an oven at a constant temperature of 60 °C. The titanium foils and rods were immersed in NaOH solution (5 M) at 80 °C for 1 day, and the treated samples were named as AT (alkali heat-treated). Subsequently, the samples were then placed in a reactor with 10 mL hydrothermal reaction solution comprising 21.6 mM urea, 74.16 mg magnesium nitrate, 106.5 mg aluminum nitrate and 145.5 mg cobalt nitrate. The LDH coating was grown on the Ti substrate by hydrothermal treatment. After cooling down, the Ti foil was removed and placed in 1 mg/mL gallic acid overnight. The rinsing treatment was repeated several times, and the products were washed with deionized water.

2.3. Characterization of samples

The surface morphology and chemical composition of the samples were observed by scanning electron microscopy (SEM, Quattro S, Thermo Fisher Scientific), atomic force microscopy (AFM, JPK Instruments AG, Germany Nano Wizard II), X-ray photoelectron spectroscopy (XPS, ESCALAB 250Xi, Thermo Fisher Scientific), X-ray Diffraction (XRD, PANalytical X'Pert Powder, Panalytical B·V.), and energy dispersive spectroscopy (EDS), respectively. Wettability of different sample surfaces was characterized by water contact angle testing (Model 200, Future Scientific, Taiwan, China) Specifically, a liquid was dropped onto the sample surface and the image was captured by the device. Finally, the contact angle is measured by the corresponding software. Six replicates were prepared for each group and the results were expressed as mean and standard deviation. In addition, TRM100 friction testing machine was used to test the mechanical properties of different substrates under the force load of 10 N and rolling speed of 70 r/min. Tribological properties were tested under PBS lubrication at 37 °C including friction coefficient and cumulative wear. The wear rate (W, mm^3/Nm) is calculated using the following formula.

$$W = \frac{m}{\rho \times N \times S}$$

In the formula, m is the cumulative wear mass in mg, ρ is the LDH density ($\rho = 0.35$ mg/mm^3), N is the loading force (10 N), and S is the wear distance (m) during the test.

2.4. Ion release analysis

Ti, Ti-LDH and Ti-LDH/GA were treated with PBS solution (5 mL) at 37 °C for 1, 3, 7, 14, 21 and 30 days. The incubation solutions were extracted and equal volume of new PBS solutions were added at different time intervals. Finally, to analyze the Mg^{2+} and Co^{2+} release from various substrates, the collected samples were centrifuged and analyzed separately by plasma atomic emission spectrometry (ICP-AES; Vista AX, Varian, USA).

2.5. Biological response of HUVECs on Ti-LDH/GA surface in vitro

2.5.1. Viability and morphology of HUVECs

We inoculated human umbilical vein endothelial cells (HUVECs) on different titanium substrates to assay the viability of the cells. After 1 and 3 days of incubation, the cells on titanium substrates were washed 3 times with PBS and then incubated with 200 μL cck8 solution (cck8: medium = 1:9) for 4 h at 37 °C protected from light. Then, the cck8 mixture was collected and detected at 490 nm using an enzyme marker (Bio-Rad 680).

After seeding endothelial cells on the surface of different samples, the cells were further incubated for 24 h and the culture medium was discarded, PBS washed three times, and 100 μL of FDA (100 μM) and 100 μL of PI (100 μM) were added to stain the cells for 10 min at room temperature and protected from light, and finally, all samples were observed by inverted fluorescence microscopy imaging.

After 24 h of continuous culture on different titanium substrates, the samples were fixed with 4 % paraformaldehyde at 4 °C for 30 min and permeabilized with 0.2 % Triton X-100 for 2 min. Then, samples were treated with rhodamine-labeled ghost-closed peptide and Hoechst 33,258 at 4 °C under light-protected conditions. Finally, different cell morphologies on the samples were observed using a laser confocal microscope (CLSM, TCS SP5, Leica, Germany).

2.5.2. Migration of HUVECs

Wound healing assays were used to study the migration behavior of HUVECs on different titanium groups. HUVECs were inoculated onto different titanium substrates as described above. When the cell confluence on the different substrates reached 80–90 % confluence, the cell monolayers were scraped using P20 pipette tips and the collected samples were rinsed with PBS. After that, the cells were separately cultured with medium containing 1 % fetal bovine serum for another 12 h. Then, the cells were stained with rhodamine ghostwriter and Hoechst 33,258. Finally, all samples were observed with a microscope (DMI 600 B Leica).

The effect of the material on the migration of HUVECs was further assessed using transwell analysis. The transwell chambers (8 μm pore size, Corning, USA) were placed in 24-well plates while the cells were cultured in the upper chamber of 600 μL medium containing 1 % fetal bovine serum. After 12 h of incubation, the remaining cells in the upper chamber were wiped with a clean gauze. Cells migrated into the lower chamber were then stained with crystal violet. All samples were observed by an optical microscope (Olympus).

2.5.3. Immunofluorescence staining assay

Cell immunofluorescence staining was performed to detect the expression of VEGF, iNOS and HIF-α. Briefly, HUVECs were cultured on the surface of different samples for 24 h, fixed with paraformaldehyde for 30 min, and then permeabilized with 200 μL of 0.2 % Triton X-100 for 3 min. After blocking with 1 % bovine serum albumin solution for 1 h, the samples were incubated with rabbit monoclonal antibody overnight. Subsequently, the cells were incubated with Alexa Fluor488 secondary antibody for 1 h, and the nuclei were stained with Hoechst 33,258. Finally, anti-fluorescence burst fixation medium was added, and samples were mounted on glass slides for observation by a laser confocal microscope.

2.5.4. Expression of angiogenesis-related genes and proteins

Polymerase chain reaction was used to analyze the expression of angiogenesis-related genes in endothelial cells after incubation on the surfaces of different materials. HUVECs were inoculated on the sample surfaces for 7 days, and total RNA was extracted using the RNA kit from Omega, USA. Total RNA was reverse transcribed into cDNA using the PrimeScrip RT kit (Takara, China). The synthesized cDNA was then mixed with SYBR Green Mastermix and primers to quantify the expression levels of target genes. These specific primers (Table S1) were obtained from Sangon (China). The two-step cyclic amplification protocol was: 3 s at 95 °C, 5 s at 95 °C for 45 cycles, and 30 s at 60 °C. The mRNAs of the above genes were normalized by the GAPDH gene level.

HUVECs were cultured on different titanium substrates for 7 days. Cells were then washed three times with PBS, lysed with RIPA lysis buffer containing 1 mM phenylmethylsulfonyl fluoride, and processed with sample buffer at 100 °C for 10 min. Protein concentrations were equalized after measurement with a BCA protein assay kit. Proteins were then separated by 10 % SDS polyacrylamide gel electrophoresis and transferred onto PVDF membranes at 300 mA for 70 min. The membranes were blocked at room temperature with 5 % non-fat milk and

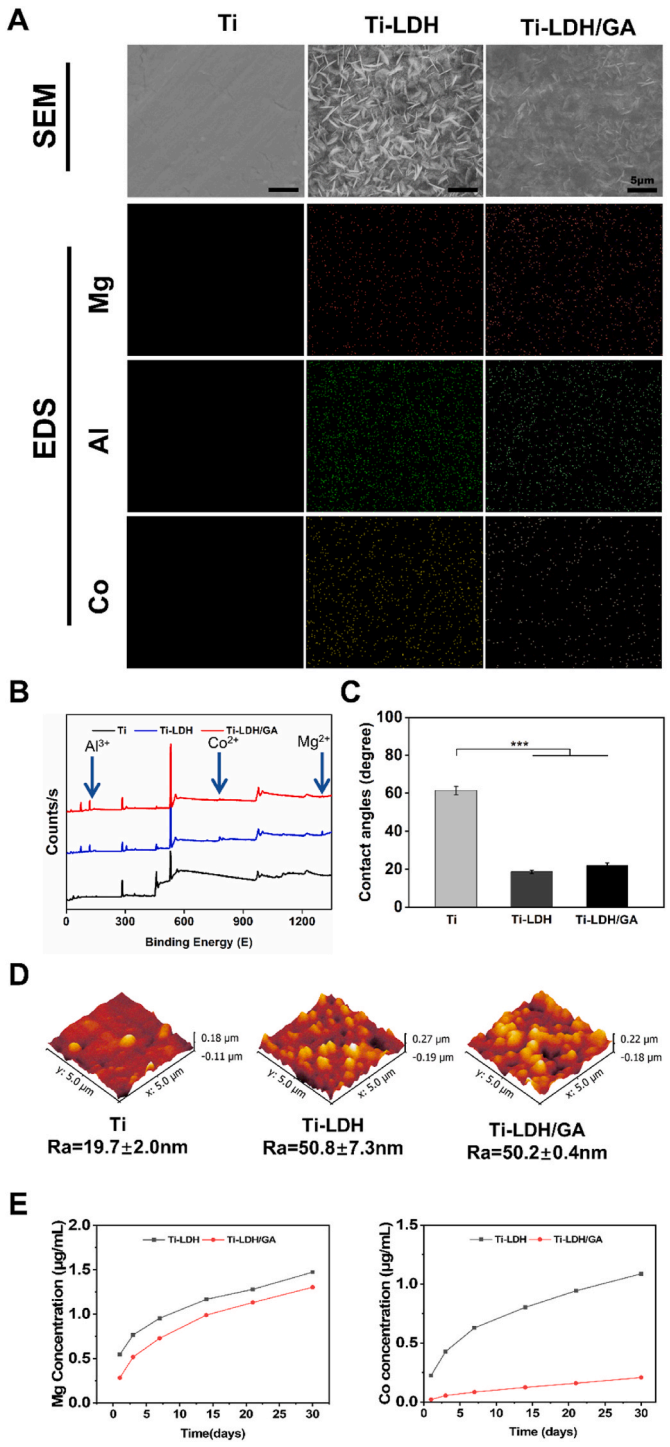

Fig. 2. (A) SEM images and EDS images of different substrates (scale bar: 5 μm). (B) XPS patterns of different samples. (C) Water contact angles and (D) AFM images of different substrates. (E) Release profiles of Mg^{2+} and Co^{2+} released from Ti-LDH and Ti-LDH/GA under different incubation conditions. N = 3, ***p < 0.001.

TBST for 1 h, followed by overnight incubation at 4 °C with primary antibody at a 1:1000 dilution. Secondary antibody incubation was done at room temperature for 1 h, followed by five washes with TBST. Membranes were imaged using the Bio-Rad ChemiDoc MP imaging system to analyze protein expression.

2.5.5. Tube formation assay

We examined the ability of endothelial cells to generate blood vessels on the surface of different samples using microtubule formation assay. Ti-LDH and Ti-LDH/GA were placed in 24-well plates with serum-free medium and seeded with HUVECs as described above, afterwards the supernatant was collected after incubation in an incubator for 24 h by centrifugation. 96-well culture plates and sterile tips were pre-chilled at −20 °C for 24 h. Meanwhile, MATRIGEL (BD MATRIGEL™ 356,234, USA) was dissolved at 4 °C. All subsequent experiments were performed on ice. A 96-well plate was coated with 50 μL of matrix gel per well and incubated at 37 °C for 30 min in an incubator to allow the matrix gel to solidify. Each well was added with 1 mL of sample extract combined with 1×10^4 HUVECs, and the culture continued for 8 h. The vascular structures were observed under an inverted microscope.

The synergistic index between Co and Mg ions were calculated using the following formula:

$$CI = \frac{(D)_1}{(D_x)_1} + \frac{(D)_2}{(D_x)_2}$$

Herein, the items $(D_x)_1$ and $(D_x)_2$ are the Co and Mg concentrations that are required to achieving the same pro-osteogenesis and pro-angiogenesis potency using Co/Mg combinations. $(D)_1$ and $(D)_2$ are the concentrations of Co and Mg in the optimal Co/Mg combinations. The pro-osteogenesis and pro-angiogenesis effects under different conditions were measured via ALP assay and tube formation assay, respectively.

2.6. Cell viability and morphology of MSCs

Mesenchymal stem cells (MSCs) were inoculated on different titanium substrates and the activity of the cells on the surface of the material was investigated using CCK-8 assay. After 1 and 3 days of incubation, the cells on the titanium substrates were washed three times with PBS and then incubated with 200 μL CCK-8 solution (CCK-8: medium = 1:9) for 4 h at 37 °C in dark environment. Then, the sample solutions were collected and detected at 490 nm using an enzyme marker (Bio-Rad 680). After 24 h of culture on different titanium substrates, samples were fixed with 4 % paraformaldehyde at 4 °C for 30 min and permeabilized with 0.2 % Triton X-100 for 2 min. Then, samples were treated with rhodamine-labeled ghost-closed peptide and Hoechst 33,258 at 4 °C under dark conditions. Finally, cell morphologies on the samples were observed using a laser confocal microscope (CLSM, TCS SP5, Leica, Germany).

2.7. Evaluation on the crosstalk between vascularization and MSC osteogenic differentiation

2.7.1. Collection of conditioned medium

First, HUVECs cells were cultured on different samples for 2 days. Next, the medium was collected and centrifuged for 15 min. Then, the supernatant was mixed with DMEM medium at a volume ratio of 1:1 to form conditioned medium for MSC culture.

2.7.2. ALP activity assay

MSCs were cultured in different conditioned media for 4 and 7 days, respectively, and then stained with BCIP/NBT alkaline phosphatase staining kit and imaged with Olympus MVX10 MacroView (Japan). Then, cell lysis in different groups were prepared for quantitative analysis. Total intracellular protein and alkaline phosphatase during cell lysis were measured with the BCA kit and alkaline phosphatase assay kit, respectively. Alkaline phosphatase activity was expressed as micrograms of *p*-nitrophenol per milligram of total intracellular protein. Finally, the absorbance of the samples at 490 nm was measured using a BioRad-type microplate reader (Bio-Rad, USA).

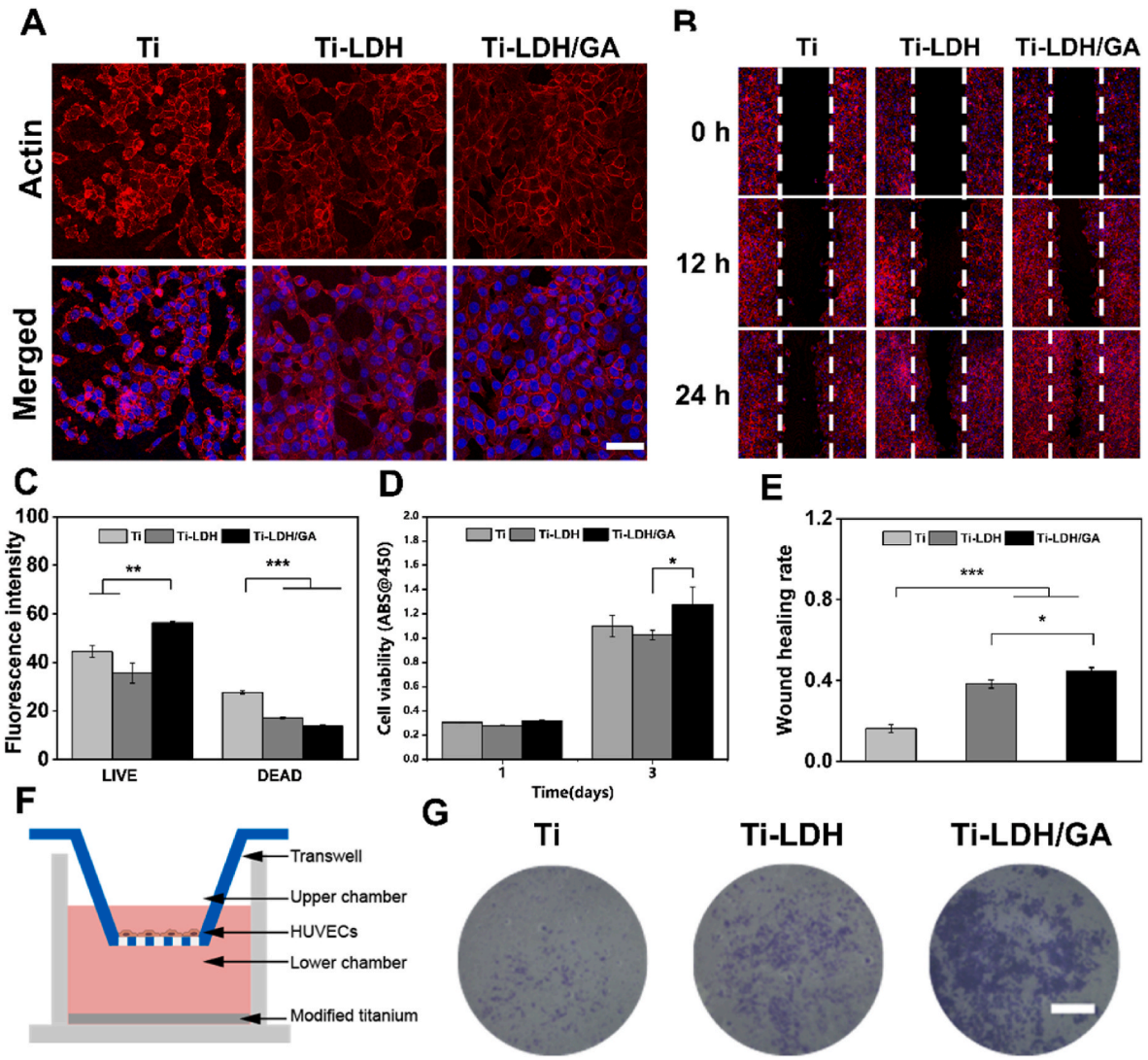

Fig. 3. (A) Morphology of HUVECs on the surface of different materials (scale bar: 50 μm). (B) The fluorescence image of endothelial cell migration after 12 h of incubation in wound healing assay (scale bar: 500 μm). (C) Quantitative analysis of cell viability according to panel fluorescence. (D) Cell viability of HUVECs after inoculation onto different substrates. (E) Statistical analysis of wound healing rate under different conditions. (F) Schematic diagram of transwell assay setup. (G) Optical imaging showing the migration of endothelial cells in the transwell assay for 12 h (scale bar: 200 μm). N = 4, *p < 0.05, **p < 0.01, ***p < 0.001.

2.7.3. Mineralization assay

The mineralization levels of MSCs were investigated using different conditioned media. MSCs were fixed with 4 % paraformaldehyde after 14 and 21 days of incubation on the surface of different samples and stained with alizarin red (pH 4.1). The samples were washed with deionized water and then observed using an Olympus light microscope (MVX10, Olympus). Afterwards, 10 % (v/v) acetic acid solution was added and the solution was incubated for 20 min. Then, cells were scraped off the material and heated in an 85 °C water bath for 10 min. The supernatant was collected by centrifugation after treatment with 10 % ammonia. Finally, the absorbance value at 405 nm was detected using a BioRad-type microplate reader (Bio-Rad, USA).

2.7.4. qPCR analysis

Finally, the expression of genes related to osteogenic differentiation of MSCs on the surface of different materials was analyzed by polymerase chain reaction. After inoculating MSCs in different conditioned media for 7 days, total RNA was extracted using RNA kit (Omega, USA). Total RNA was reversely transcribed into cDNA using PrimeScrip RT kit (Takara, China). Synthesized cDNA was then mixed with SYBR Green Mastermix and primers to quantify the expression of target genes. These specific primers were obtained from Sangon (China). The two-step cyclic amplification protocol was: 3 s at 95 °C, 5 s at 95 °C for 45 cycles, and 30 s at 60 °C. The mRNAs of the above genes were normalized by GAPDH gene level.

2.8. In vivo experiments

Sprague-Dawley (SD) rats weighted 200–250 g were provided by Chongqing Medical University, and all animal experiments were approved by the Ethics Committee of the Army Medical University (Chongqing, China, SYXK-PLA2120031). All rats were provided by the same supplier, were of comparable age/weight, and were of the same sex. We used 15 SD rats in the study experiments. A total of three groups were tested *in vivo*, with each group containing five SD rats (n = 5). All rats were kept by a third-party experimental center for 3 days prior to the experiments, during which time only water and food were provided. Different implants of sterile Ti, Ti-LDH and Ti/LDH-GA, labeled 1, 2 and 3, were prepared as described above and given to the third-party technicians in advance. SD rats were injected intraperitoneally with 0.3 mL/100 g of 2 wt% sodium barbiturate solution prior to implantation. Then, the third-party technician used a sterile scalpel (Wuhan Golden Light

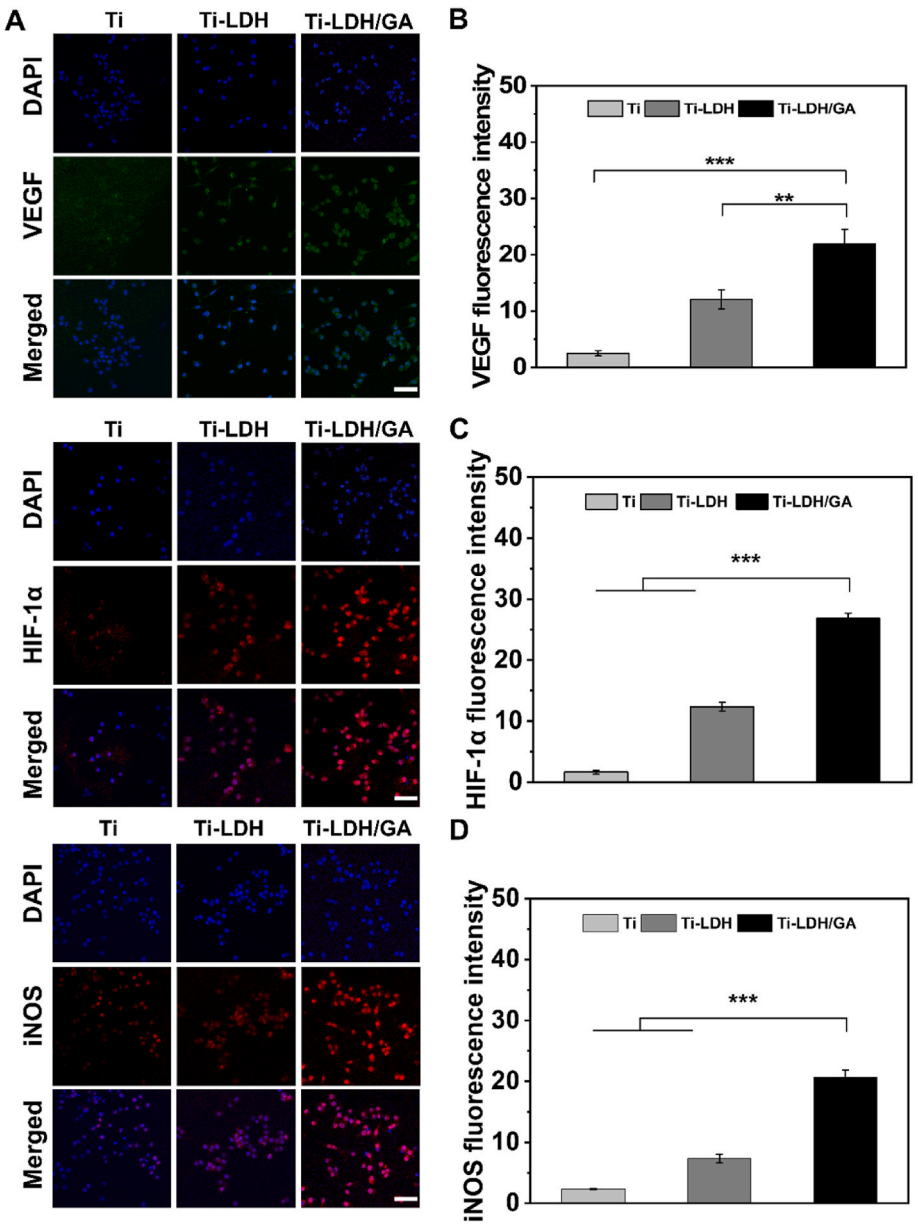

Fig. 4. (A) Immunofluorescence staining results showing the expression of various vascularization related markers including VEGF, iNOS and HIF-1α. (B–D) Corresponding quantitative analysis results. N = 4, **p < 0.01, ***p < 0.001, scale bar: 50 μm.

Medical Technology Co., Ltd.) to expose the end of the femur, and used a surgical drill to form a cylindrical defect between the epiphysis and the diaphysis. Finally, the numbered material was inserted into the defect site and the wound was closed with sutures. The authors had no knowledge of the randomized dosing procedure. On the first, second, and third postoperative days, 100 μL of penicillin (2×10^5 U/mL) was injected into the muscle surrounding the wound in each rat. After surgery, the rats were able to move normally. After feeding for one month after surgical implantation, the experimental rats were euthanized, and the rat femur specimens were collected and fixed with 4 % paraformaldehyde for 3 days, and the residual fixation was rinsed with PBS to observe the osteogenesis around the implant in SD rats by micro-computed tomography (Micro-CT); SCAN Viva CT40 V^6.1 software was used to further quantify the mass of new bone around the implant (0.6 mm). The peri-implant vascularization and osteogenesis-related proteins (CD31, OPN, OCN and COI–I) were analyzed by immunohistochemical staining tests 1 month after the implantation procedure, as previously reported. To assess new bone formation around the defect, we stained the sections with H&E and Masson kits. Then, sections were immunohistochemically stained to illustrate the expression of bone formation marker proteins OCN, collagen type I (COL-I), and OPN. Finally, all sample sections were photographed and observed with an Olympus inverted microscope.

2.9. Statistical analysis

Quantitative data are expressed as mean ± standard deviation (SD). Statistical analysis was carried out through one-way analysis of variance (ANOVA) in Origin Pro (version 2023) with confidence levels set at 95 % and 99 %. All data are expressed as mean ± SEM (standard error of the mean).

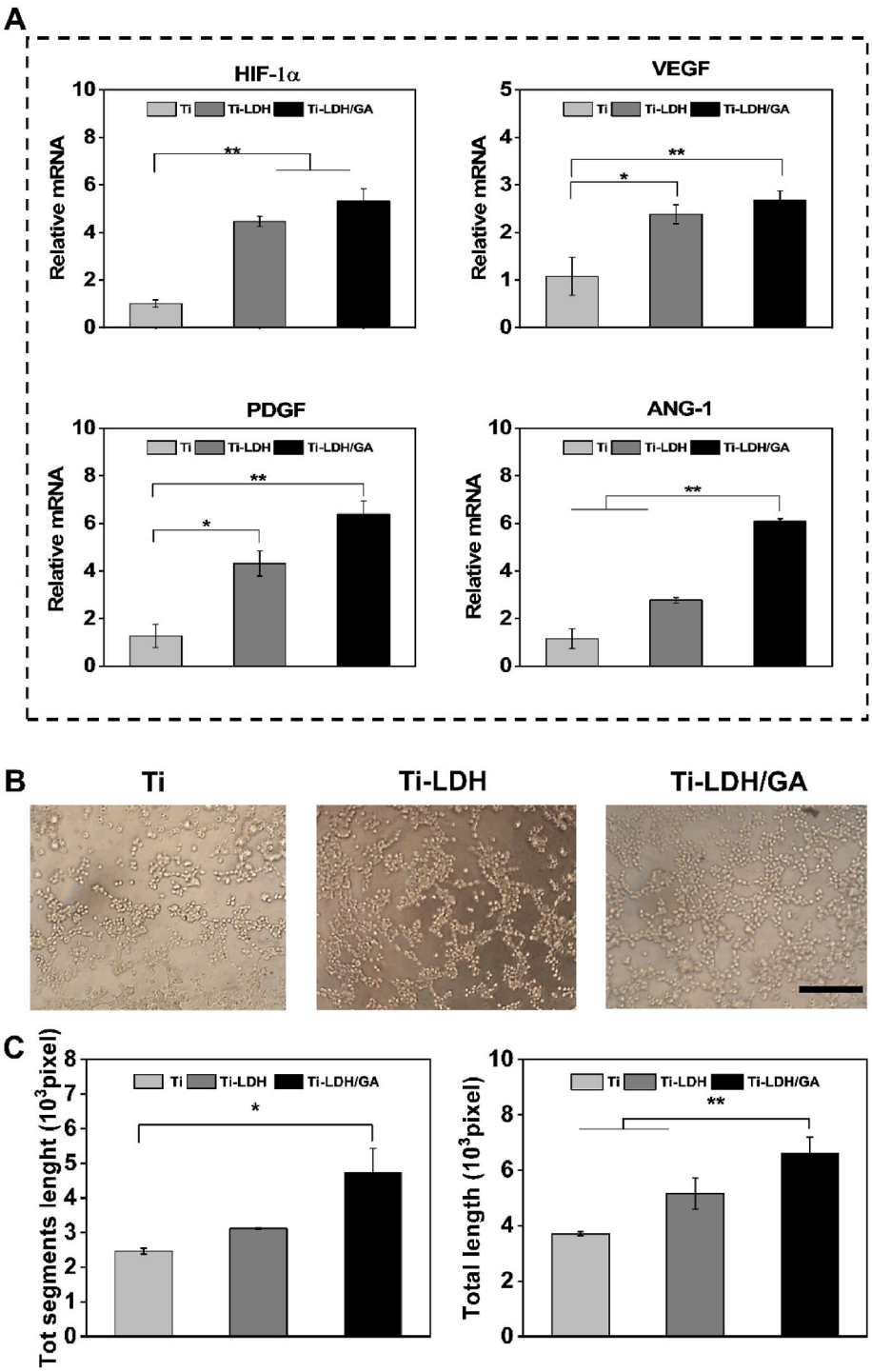

Fig. 5. (A) Expression levels of various vascularization related genes including HIF-1α, VEGF, PDGF, ANG-1 in HUVECs after treatment with different samples. (B) Optical imaging showing the tube formation by HUVECs after different treatment. (C) Quantitative analysis of HUVEC tube formation. N = 4, *p < 0.05, **p < 0.01.

3. Results and discussion

3.1. Material characterization

In this study, we employed a high-pressure hydrothermal system to generate Co-doped Mg–Al LDH structures on the surface of titanium, followed by forming a gallic acid layer on top of the LDH structures through chelating with the metal ions. SEM analysis (Fig. 2A) revealed that pure Ti exhibited relatively smooth morphology, while Ti-LDH displayed a homogeneous hexagonal lamellar surface structure with minor size differences. LDH-GA showed a relatively uniform coating on the surface that blurred the lamellar structure of LDH. EDS analysis was then carried out to determine the chemical composition of the lamellar structure and the coating. As indicated in Fig. 2A, only Ti signals observed on the surface of pure Ti, while Mg, Al and Co signals appeared in Ti-LDH and Ti-LDH/GA samples. A similar trend was observed in the XPS analysis results (Fig. 2B). It is notable that the intensity of metal signals on the Ti-LDH/GA surface was lower than that of LDH, which could be explained by the addition of the gallic acid coating. Based on previous research, it is known that the hydrophilicity of the biomaterial

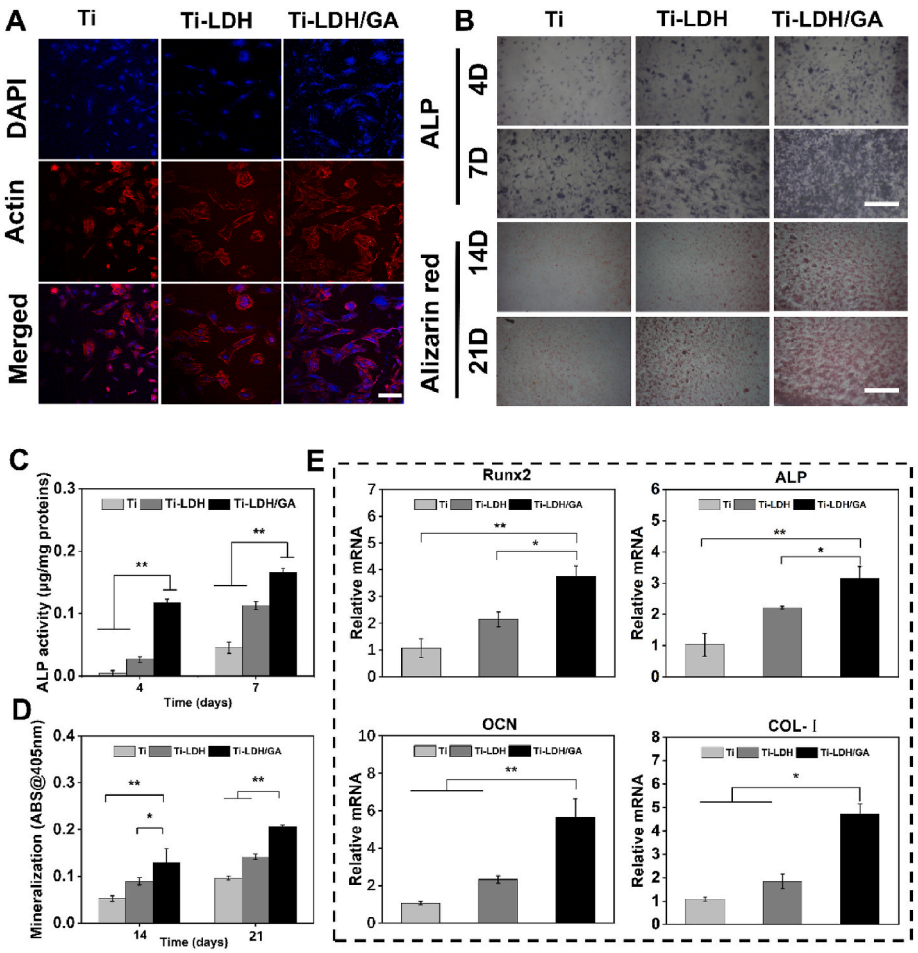

Fig. 6. (A) MSC morphologies after inoculation onto different implants (scale bar: 100 μm). (B) ALP and Alizarin red staining images of MSCs after different treatment (scale bar: 500 μm). (C) Quantitative analysis of ALP activity in MSCs after different treatment. (D) Quantitative analysis showing the mineralization levels of MSCs after different treatment. (E) Expression of osteogenic differentiation-related genes in MSCs after culturing onto different samples for 7days, including Runx2, ALP, OCN and COL-I. N = 3, *p < 0.05, **p < 0.01.

surface significantly affects its interaction with ambient cells [38,39]. Therefore, we examined the hydrophilicity (Fig. 2C) of various titanium-based materials. The contact angle of pure Ti was 59°, which decreased to 20° after the formation of LDH structure on the Ti surface and supported the good hydrophilicity of LDH. The addition of GA coating did not induce significant changes on the contact angle values. Additionally, we assessed the surface roughness of Ti, Ti-LDH, and Ti-LDH/GA using AFM (Fig. 2D) and found that the surface roughness of Ti was lower than that of Ti-LDH and LDH-GA, which was caused by the formation of the LDH coating on the Ti surface. There was no significant difference in the surface roughness between Ti-LDH and Ti-LDH/GA. Overall, these data collectively confirmed the successful formation of LDH-based functional coating on Ti surface with robust quality.

To further assess the stability of LDH on the titanium surface, friction tests (Figure S3A) were conducted in an aqueous environment at a load of 10 N and a speed of 70r/min, representing the mechanical stress experienced by bone implants in the body [48]. Compared with the unmodified Ti surface, both Ti-LDH and Ti-DH/GA groups exhibited significantly higher friction coefficients ($P < 0.05$), which was attributed to the relatively higher roughness of the surface coating and typical for surface engineered Ti implants in previous reports [49]. This is also consistent with the AFM observation. In addition, we calculated the wear rate of the Ti-based substrate (Figure S3B) based on cumulative weight loss to indicate the shear bonding strength of the coatings. Specifically, under a load of 10 N, the implant exhibited a wear rate of 0.01713679 mm^3/Nm, which was at a comparable level to the wear resistance in established reports [50,51]. These findings evidently suggested the robust mechanical resilience of the Ti-LDH/GA implants under physiological conditions for *in vivo* application.

3.2. Ion-release behavior from implant surface

In order to study the release behavior of metal ions, different titanium-based materials were incubated in T-PBS solution for different periods. As shown in Fig. 2E, both Ti-LDH and Ti-LDH/-GA showed continuous release of metal ions from the surface; however, the release rates of Mg and Co on the surface of Ti-LDH/GA were slower than those of the LDH group, attributing to the stabilization effect of gallic acid chelation. Notably, Co ions have relatively slower release rate than Mg ions, which is attributed to the greater net negative charge of Co ions and may significantly enhance the stability of the Co-GA coordination complex, thereby impeding the liberation of Co ions [52,53]. This is also consistent with dissociation constants and binding energies of Co and Mg ions with the metal chelating moieties in GA species [54]. The continuous Mg release at steady rates could not only ensure its pro-angiogenesis activity [55] but also prevent the Mg-associated side effects, as previous insights confirmed that high concentrations of magnesium ions prevented the uptake of calcium ions into bone healing-related cells, which may negatively affect bone mineralization and maturation and thus impede bone regeneration [56]. On the other hand, Co ions can also stabilize HIF-1α and contribute to the pro-angiogenesis effects [57]. Therefore, it is anticipated that the

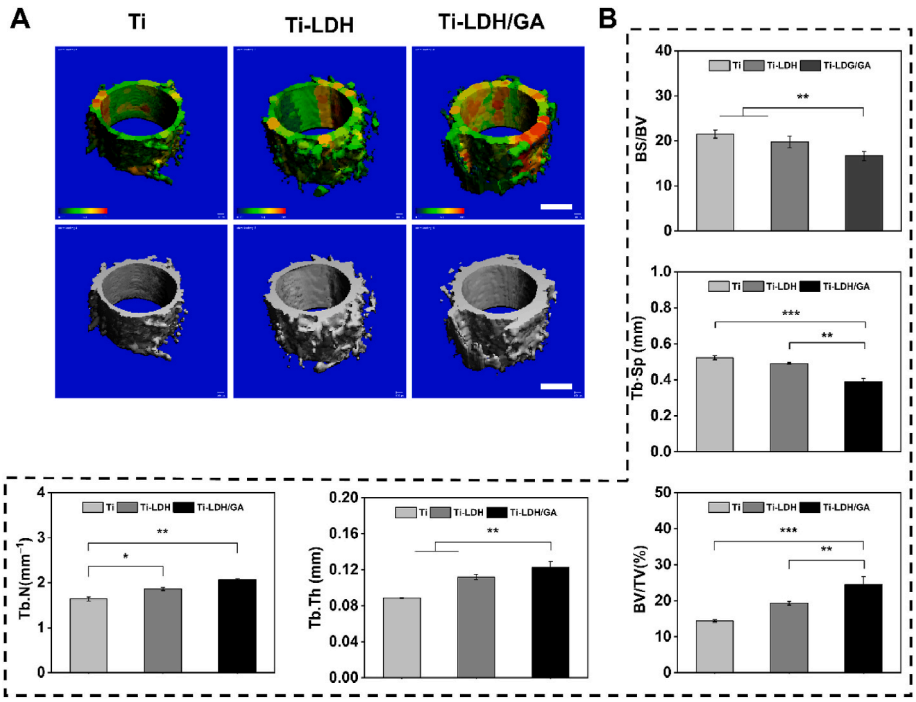

Fig. 7. (A) Micro-CT analysis showing peri-implant new bone formation in different groups (scale bar: 500 μm). (B) Quantitative analysis of new bone tissue in different groups (BS/BV, Tb. Sp, BV/TV, Tb·Th, and Tb·N). N = 5, *p < 0.05, **p < 0.01, ***p < 0.001.

controlled release of Mg and Co ion combination could cooperatively promote peri-implant angiogenesis while avoiding side effects associated with excessive Mg ions.

We then carried out comprehensive analysis to determine the concentration dependence of Mg-associated biofunctions. In terms of cytotoxicity (Figure S4A), our results showed that Mg ions did not show obvious toxicity when their concentration was below 1000 μg/mL. Meanwhile, analysis results with ALP activity assay kits (Figure S4B and S4C) demonstrated that Mg ions in the ranges of 0.1 μg/mL to 100 μg/mL significantly boosted the alkaline phosphatase activity in bone marrow mesenchymal stem cells for stimulating their osteogenic differentiation. Furthermore, tube formation analysis (Figure S4D) indicated that Mg ions within the concentration range of 0.1 μg/mL to 10 μg/mL could effectively promote the angiogenetic potential of HUVECs. These data were consistent with observations in previous reports [58–61]. Interestingly, the accumulative concentration of released Mg ions from Ti-LDH/GA material was in the range of 0.5 μg/mL to 1.5 μg/mL within the treatment period, further verifying of our hypothesis that Ti-LDH/GA implants could release adequate amount of Mg ions to promote new bone formation while avoiding Mg-associated toxicities through controlled Mg release.

3.3. *Biological response of endothelial cells on to biofunctional Ti implants*

The pro-angiogenesis capacity of the implants was first investigated by monitoring the growth of HUEVCs after culturing on different titanium-based materials. The viability of HUVECs on Ti-LDH/GA surface after one day and three days of culturing was higher than that of the control group (Fig. 3D, Figure S1)), which was consistent with the live-dead cell staining results (Fig. 3C). The cell scratch migration assay showed that HUVECs in the Ti group showed only modest migration at 12 h and a lower wound healing rate (Fig. 3E). Compared with the control group, the Ti-LDH/GA group showed the greatest extent of HUVEC migration to the scratch area (Fig. 3B). Notably, Ti-LDH group showed reduced viability than pristine Ti and Ti-LDH/GA. This is probably associated with the needle-like lamellar morphology of the generated LDH species, which has also been reported in multiple recent publications [62–64]. Indeed, the surface morphology of implant coating has been identified as an important mediator of the viability of adherent cells on implant surface, and the needle-like lamellar LDH may impair HUVEC viability in addition to the pro-migration effect of the released divalent metal ions [65–67]. Therefore, the surface modification of GA could enhance the smoothness of the lamellar surface to reduce their potential negative impact on the viability of adherent cell while retaining the pro-migration effect of incorporated metal ion species [68,69]. Transwell invasion assay confirmed that the migration ability of HUVECs in the Ti-LDH group was elevated compared with the Ti group, while HUVECs in the Ti-LDH/GA group showed the strongest migration ability (Fig. 3G). To further investigate the treatment-induced changes in expression of angiogenesis-related proteins in endothelial cells, we performed immunofluorescence staining of the HUVECs and found that the fluorescence intensity of angiogenesis-associated proteins including HIF-1α, iNOS and VEGF in the Ti-LDH/GA group was evidently higher than Ti and Ti-LDH groups (Fig. 4A). Quantitative analysis of the immunofluorescence data (Fig. 4B) showed that the expression of HIF-1α in the Ti-LDH/GA group was 16.4-fold and 2.16-fold higher than that of Ti and Ti-LDH, respectively. The expression of iNOS and VEGF proteins in Ti-LDH/GA-conditioned endothelial cells exhibited similar trends. Similar trends were also detected for the gene levels of those angiogenesis-related markers (VEGF, HIF-α, ANG-1, PDGF) in cells cultured on different materials using PCR experiments (Fig. 5A) and further coincided with WB data on the associated protein expression levels (Figure S5). These observations were consistent with previous insights that activating the VEGF signaling can notably promote angiogenesis capacity of HUVECs.

Finally, we performed *in vitro* angiogenesis assays (Fig. 5B) to evaluate the angiogenic potential of HUVECs on different titanium-based materials. The results indicated that cells from Ti-LDH/GA group had the highest angiogenic potential than the other two groups, which was further validated via quantitative analysis (Fig. 5C) on vessel length. Angiogenesis assay results also showed that Ti/GA has higher pro-angiogenesis capacity (Figure S6C) than pristine Ti samples but lower than Ti-LDH and Ti-LDH/GA, which could be explained by pro-adhesion

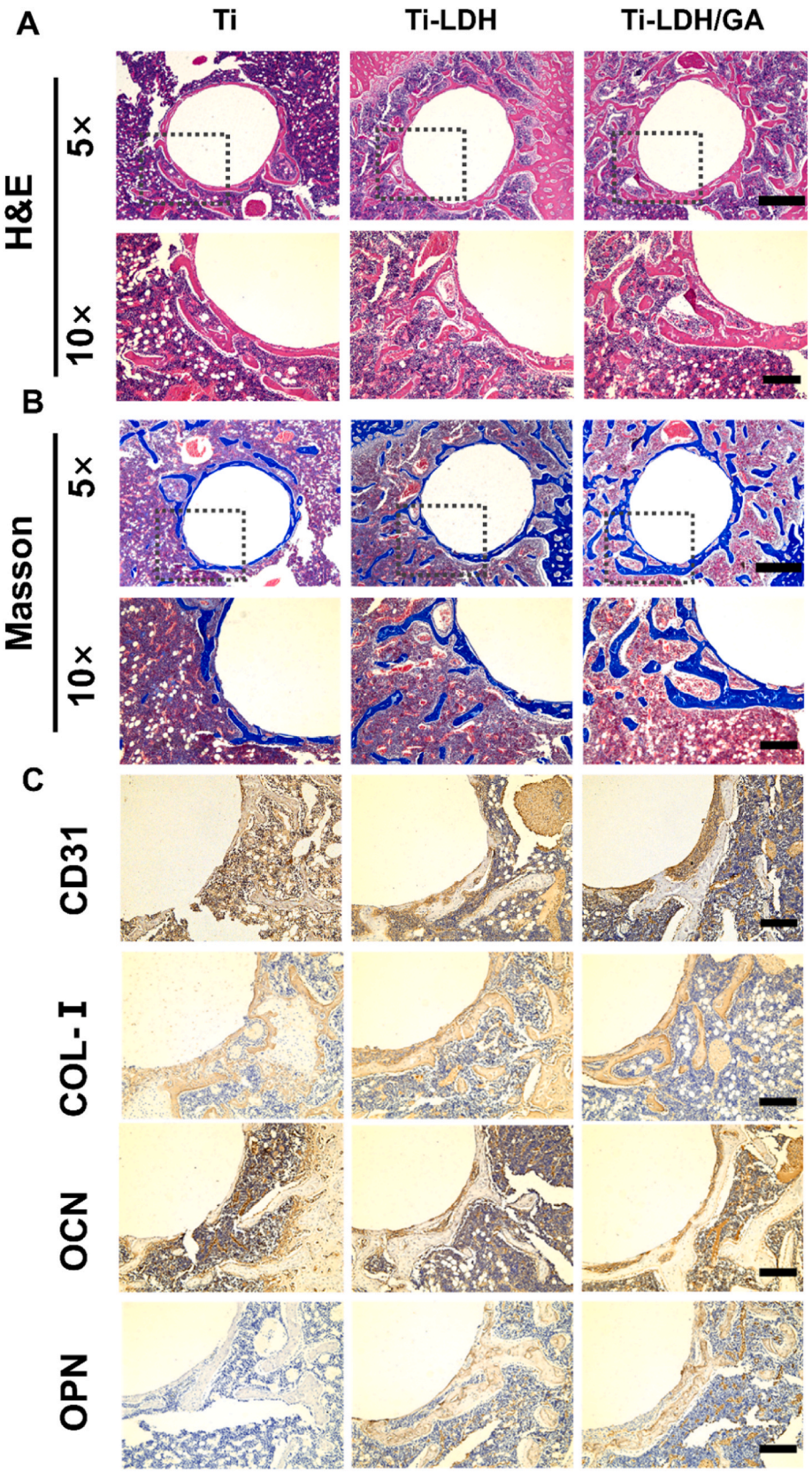

Fig. 8. (A) H&E staining of new bone tissues in different groups (scale bar for top row: 500 μm. Bottom row: 200 μm); (B) Masson staining of new bone tissues in different groups. (C) Immunohistochemical staining of CD31, COL-I, OCN and OPN in the bone tissues from different groups (scale bar: 200 μm).

capacity of GA in recent reports [68,69] as well as the lack of bioactive divalent metal ions. The observations were consistent with previous insights on the pro-angiogenesis activity of Co and Mg ions [70,71]. Indeed, Mg^{2+} induces nitric oxide production in endothelial cells, which may combine with the Co-stimulated HIF signaling to promote angiogenesis. These merits acted in a cooperative manner to enhance the capacity of Ti-LDH/GA to promote the angiogenic function of HUVECs, which is beneficial for new bone formation at bone-implant interface.

3.4. Evaluation on implant-promoted osteogenic differentiation of MSCs

CCK-8 assay was first used to evaluate the viabilities of MSCs on different titanium-based materials. After one day of culture, Ti-LDH exhibited modest inhibitory effect to the inoculated MSCs, whereas Ti-LDH/GA showed significantly higher cytocompatibility than the other two groups. This trend was also observed after three-day culture (Figure S2). We speculate that this could be due to the release control capability of GA layer that could prevent the excessive burst release of Mg and Co ions and thus avoid the associated acute toxic effects. Following 24 h of inoculation on implant surface, the cytoskeleton and nucleus of MSCs were re-stained with rhodamine-labeled ghost-closing peptide and Hoechst 33,258 to assess the cellular status. As depicted in Fig. 6A, MSCs on Ti-LDH and Ti-LDH/GA surfaces displayed numerous filopodia-like pseudopods, indicating that the high roughness of these materials was more conducive to cell adhesion. Additionally, cells on the Ti-LDH/GA surface exhibited superior spreading and extension. These observations were consistent with previous studies that polyphenolic species could substantially alter surface properties of titanium implants such as roughness and surface affinity, leading to improved cell adhesion and spreading [72].

We then investigated the alkaline phosphatase expression in MSCs cultured in various conditioned media, which is a marker of early osteogenic differentiation. The ALP staining results demonstrated Ti-LDH/GA induced higher expression of ALP than both Ti-LDH and Ti after 4 and 7 days of culture (Fig. 6C). Alizarin red staining and mineralization assays on inoculated MSCs revealed a similar trends after 14 and 21 days of culture (Fig. 6C). Pristine GA coating also showed modest promotional effect on osteogenic differentiation (Figure S6A and S6B), confirming that incorporated GA has moderate pro-angiogenesis and osteogenesis capacities while necessitating the presence of LDH for enabling efficient bone healing. To further determine the osteogenic differentiation levels of MSCs on different titanium surfaces, we examined the expression of osteogenesis-related genes, namely osteocalcin (OCN), Runt-related transcription factor 2 (Runx2), alkaline phosphatase (ALP), and collagen type I (COL-I). As illustrated in Fig. 6E, Ti-LDH/GA considerably increased the expression of all these osteogenesis-related genes in MSCs, which was 3.05, 5.36, 4.38, and 3.38 times higher than the Ti surface, respectively. The findings suggest that Ti-LDH/GA enhances the osteogenic differentiation of MSCs. This phenomenon may be attributed to multiple factors. It is well established that Mg ions could enhance osteogenesis of MSCs via the stimulating Notch and Wnt/β-catenin signaling pathways as well as interacting with PI3K/Akt to elevate ALP and BMP levels for boosting bone growth. Additionally, Mg and Co ions could promote blood vessel formation through stimulating VEGF secretion to accelerate bone healing [36,73,74]. Based on Loewe Additivity model (Figure S7), Co and Mg ions have a synergistic index of 0.15453 and 0.27150 in the context of pro-angiogenesis and osteogenesis effects, evidently confirming the synergy in between.

3.5. In vivo experiments

The pro-bone healing effect of the biofunctional implants was finally evaluated *in vivo* using SD rat models bearing bone defects. One month following implantation, Micro-CT analysis was conducted to evaluate new bone formation around the different implant interfaces (Fig. 7A). Compared to pure titanium, Ti-LDH/GA showed greater new bone (gray parts) and trabecular bone (red) formation. Quantitative analysis revealed that Ti-LDH/GA had a significantly higher ratio of bone volume to total volume (BV/TV), trabecular bone thickness (Tb·Th), and trabecular bone number (Tb·N) as well as a lower trabecular bone gap (Tb.Sp) compared with other groups (Fig. 7B). H&E staining and Masson staining results demonstrated that Ti-LDH/GA induced a significant increase in new bone formation than Ti and Ti-LDH implants (Fig. 8A and B). Immunohistochemical staining showed that Ti-LDH/GA implants expressed higher levels of CD31, osteopontin (OPN), collagen type I (COL-I), and osteocalcin (OCN) than Ti-LDH and Ti implants in new bone tissue (Fig. 8C). In addition, immunofluorescence staining for CD31 and VEGF (Figure S8) also showed that the columnar tubes and arches around the Ti-LDH/GA implant had high expression levels of CD31 and VEGF, clearly confirming the expansion of blood vessels in the peri-implant area. These results suggest that Ti-LDH/GA has greater potential to promote peri-implant vascularization and new bone formation to enhance implant osseointegration and defect healing. Furthermore, we did not observe obvious pathological alterations or damages in the peri-implant region, again validating our hypothesis that the controlled and sustained release of metal ions from the functional coating could facilitate new bone formation with optimal safety.

4. Conclusion

Extending from the important role of divalent metal ions in angiogenesis and osteogenesis process, here we reported a Co-doped Mg–Al LDH coating on Ti surface with chelated gallic acid layer as ion release gatekeepers via hydrothermal reaction, which enabled controlled and sustained release of Mg and Co ions from implant surface to promote implant osseointegration and defect healing. The controlled and sustained release of Mg and Co ions from Ti-LDH/GA surface can effectively induce angiogenesis and osteogenic differentiation of adhered cells after implantation through HIF signaling, ultimately leading to the formation of abundant new bone tissue around the implant. This research provides an efficient approach for the development of novel functional titanium-based orthopedic implants.

CRediT authorship contribution statement

Xiaodong Chen: Data curation, Formal analysis. **Shuohan He:** Data curation, Formal analysis, Writing - review & editing. **Yilong Dong:** Data curation, Formal analysis. **Maohua Chen:** Data curation, Formal analysis. **Zengzilu Xia:** Conceptualization, Project administration, Writing - review & editing. **Kaiyong Cai:** Conceptualization, Supervision, Writing - review & editing. **Yan Hu:** Conceptualization, Supervision, Writing - original draft, Writing - review & editing.

Declaration of competing interest

The authors declare that they have no known competing financial interests or personal relationships that could have appeared to influence the work reported in this paper.

Data availability

Data will be made available on request.

Acknowledgments

This work was financially supported by National Key R&D Program of China (2022YFB3804400), National Natural Science Foundation of China (51773023, 21734002, 51825302), Natural Science Foundation of Chongqing China (CSTB2022NSCQ-MSX0488). The authors would like to thank the Analytical and Testing Center of Chongqing University for their assistance during sample characterization.

Appendix A. Supplementary data

Supplementary data to this article can be found online at https://doi.org/10.1016/j.mtbio.2023.100912.

References

[1] M. Abdel-Hady Gepreel, M. Niinomi, Biocompatibility of Ti-alloys for long-term implantation, J. Mech. Behav. Biomed. Mater. 20 (2013) 407–415, https://doi.org/10.1016/j.jmbbm.2012.11.014.

[2] L.C. Zhang, L.Y. Chen, A review on biomedical titanium alloys: recent progress and prospect, Adv. Eng. Mater. 21 (2019), 1801215, https://doi.org/10.1002/adem.201801215.

[3] M. Geetha, A.K. Singh, R. Asokamani, A.K. Gogia, Ti based biomaterials, the ultimate choice for orthopaedic implants - a review, Prog. Mater. Sci. 54 (2009) 397–425, https://doi.org/10.1016/j.pmatsci.2008.06.004.

[4] J.M. Li, J.A. Jansen, X.F. Walboomers, J. van den Beucken, Mechanical aspects of dental implants and osseointegration: a narrative review, J. Mech. Behav. Biomed. Mater. 103 (2020), 103574, https://doi.org/10.1016/j.jmbbm.2019.103574.

[5] M. Morra, C. Cassinelli, G. Cascardo, D. Bollati, R. Rodriguez y Baena, Multifunctional implant surfaces: surface characterization and bone response to acid-etched Ti implants surface-modified by fibrillar collagen I, J. Biomed. Mater. Res. 94A (2010) 271–279, https://doi.org/10.1002/jbm.a.32702.

[6] Q. Wang, P. Zhou, S. Liu, S. Attarilar, R.L. Ma, Multi-scale surface treatments of titanium implants for rapid osseointegration : a review, Nanomaterials 10 (2020) 1244.

[7] B.G. Kim, S.J. Seo, J.H. Lee, H.W. Kim, On-site surface functionalization for titanium dental implant with nanotopography: review and outlook, J. Nanomater. 2016 (2016), 3429532, https://doi.org/10.1155/2016/3429532.

[8] X. Shen, K. Hii Ru Yie, X. Wu, Z. Zhou, A. Sun, A.M. Al-bishari, K. Fang, M.A. Al-Baadani, Z. Deng, P. Ma, J. Liu, Improvement of aqueous stability and anti-osteoporosis properties of Zn-MOF coatings on titanium implants by hydrophobic raloxifene, Chem. Eng. J. 430 (2022), 133094, https://doi.org/10.1016/j.cej.2021.133094.

[9] Qingchuan Wang, Weidan Wang, Yanfang Li, Weirong Li, Lili Tan, Ke Yang, Biofunctional magnesium coating of implant materials by physical vapour deposition, Biomaterials Translational 2 (2021) 248–256.

[10] L. Bai, P. Chen, Y. Zhao, R. Hang, X. Yao, B. Tang, C. Liu, Y. Xiao, R. Hang, A micro/nano-biomimetic coating on titanium orchestrates osteo/angio-genesis and osteoimmunomodulation for advanced osseointegration, Biomaterials 278 (2021), 121162, https://doi.org/10.1016/j.biomaterials.2021.121162.

[11] X. Shen, Y. Zhang, P. Ma, L. Sutrisno, Z. Luo, Y. Hu, Y. Yu, B. Tao, C. Li, K. Cai, Fabrication of magnesium/zinc-metal organic framework on titanium implants to inhibit bacterial infection and promote bone regeneration, Biomaterials 212 (2019) 1–16, https://doi.org/10.1016/j.biomaterials.2019.05.008.

[12] Y. Bian, X. Cai, Z. Lv, Y. Xu, H. Wang, C. Tan, R. Liang, X. Weng, Layered double hydroxides: a novel promising 2D nanomaterial for bone diseases treatment, Adv. Sci. 10 (2023), https://doi.org/10.1002/advs.202301806.

[13] G. Wang, Z. Lv, T. Wang, T. Hu, Y. Bian, Y. Yang, R. Liang, C. Tan, X. Weng, Surface functionalization of hydroxyapatite scaffolds with MgAlEu-LDH nanosheets for high-performance bone regeneration, Adv. Sci. 10 (2023), https://doi.org/10.1002/advs.202204234.

[14] F. Shokrolahi, F. Latif, P. Shokrollahi, F. Farahmandghavi, S. Shokrollahi, Engineering atorvastatin loaded Mg-Mn/LDH nanoparticles and their composite with PLGA for bone tissue applications, Int. J. Pharm. 606 (2021), https://doi.org/10.1016/j.ijpharm.2021.120901.

[15] Z. Cao, L. Zhang, K. Liang, S. Cheong, C. Boyer, J.J. Gooding, Y. Chen, Z. Gu, Biodegradable 2D Fe–Al hydroxide for nanocatalytic tumor-dynamic therapy with tumor specificity, Adv. Sci. 5 (2018), https://doi.org/10.1002/advs.201801155.

[16] A. Jagtap, P.G. Wagle, E. Jagtiani, A.P. More, Layered double hydroxides (LDHs) for coating applications, J. Coating Technol. Res. 19 (2022) 1009–1032, https://doi.org/10.1007/s11998-022-00624-y.

[17] S. Cheng, D. Zhang, M. Li, X. Liu, Y. Zhang, S. Qian, F. Peng, Osteogenesis, angiogenesis and immune response of Mg-Al layered double hydroxide coating on pure Mg, Bioact. Mater. 6 (2021) 91–105, https://doi.org/10.1016/j.bioactmat.2020.07.014.

[18] M. Chen, Y. Hu, Y. Hou, M. Li, L. Tan, M. Chen, W. Geng, B. Tao, H. Jiang, Z. Luo, K. Cai, Magnesium/gallium-layered nanosheets on titanium implants mediate osteogenic differentiation of MSCs and osseointegration under osteoporotic condition, Chem. Eng. J. 427 (2022), 130982, https://doi.org/10.1016/j.cej.2021.130982.

[19] J. Zhang, C. Zhao, R. Sheng, K. Lin, X. Wang, S. Zhang, Construction of a hierarchical micro-/submicro-/nanostructured 3D-printed Ti6Al4V surface feature to promote osteogenesis: involvement of Sema7A through the ITGB1/FAK/ERK signaling pathway, ACS Appl. Mater. Interfaces 14 (2022) 30571–30581, https://doi.org/10.1021/acsami.2c06454.

[20] Q. Li, D. Wang, J. Qiu, F. Peng, X. Liu, Regulating the local pH level of titanium via Mg-Fe layered double hydroxides films for enhanced osteogenesis, Biomater. Sci. 6 (2018) 1227–1237, https://doi.org/10.1039/c8bm00100f.

[21] M. Chen, B. Tao, Y. Hu, M. Li, M. Chen, L. Tan, Z. Luo, K. Cai, Enhanced biocompatibility and osteogenic differentiation of mesenchymal stem cells of titanium by Sr-Ga clavate double hydroxides, J. Mater. Chem. B 9 (2021) 6029–6036, https://doi.org/10.1039/d1tb00805f.

[22] C. Mahapatra, P. Kumar, M.K. Paul, A. Kumar, Angiogenic stimulation strategies in bone tissue regeneration, Tissue Cell 79 (2022), 101908, https://doi.org/10.1016/j.tice.2022.101908.

[23] H. Wei, J. Cui, K. Lin, J. Xie, X. Wang, Recent advances in smart stimuli-responsive biomaterials for bone therapeutics and regeneration, Bone Res 10 (2022), https://doi.org/10.1038/s41413-021-00180-y.

[24] J.M. Fernandez, Importance of angiogenesis in the design of scaffolds for bone tissue engineering, Actual. Osteol. 16 (2020) 211–231.

[25] J.H. Huang, Q.X. Han, M. Cai, J. Zhu, L. Li, L.F. Yu, Z. Wang, G.T. Fan, Y. Zhu, J. W. Lu, G.X. Zhou, Effect of angiogenesis in bone tissue engineering, Ann. Biomed. Eng. 50 (2022) 898–913, https://doi.org/10.1007/s10439-022-02970-9.

[26] Chaozong Liu, Zhidao Xia, Additive manufacturing innovation for musculoskeletal tissue repair and regeneration: from bench to bedside, Biomaterials Translational 3 (2022) 99–101.

[27] M.A. Saghiri, A. Asatourian, F. Garcia-Godoy, N. Sheibani, The role of angiogenesis in implant dentistry part I: review of titanium alloys, surface characteristics and treatments, Med. Oral Patol. Oral Cir. Bucal 21 (2016) e514–e525, https://doi.org/10.4317/medoral.21199.

[28] J.M. Kanczler, R.O.C. Oreffo, Osteogenesis and angiogenesis: the potential for engineering bone, Eur. Cell. Mater. 15 (2008) 100–114, https://doi.org/10.22203/eCM.v015a08.

[29] U. Saran, S. Gemini, S. Chatterjee, Role of angiogenesis in bone repair, Arch. Biochem. Biophys. 561 (2014) 109–117, https://doi.org/10.1016/j.abb.2014.07.006.

[30] J. Filipowska, K.A. Tomaszewski, Ł. Niedźwiedzki, J.A. Walocha, T. Niedźwiedzki, The role of vasculature in bone development, regeneration and proper systemic functioning, Angiogenesis 20 (2017) 291–302, https://doi.org/10.1007/s10456-017-9541-1.

[31] S. Dikici, F. Claeyssens, S. Macneil, Bioengineering vascular networks to study angiogenesis and vascularization of physiologically relevant tissue models in vitro, ACS Biomater. Sci. Eng. 6 (2020) 3513–3528, https://doi.org/10.1021/acsbiomaterials.0c00191.

[32] Z. Yuan, P. Wei, Y. Huang, W. Zhang, F. Chen, X. Zhang, J. Mao, D. Chen, Q. Cai, X. Yang, Injectable PLGA microspheres with tunable magnesium ion release for promoting bone regeneration, Acta Biomater. 85 (2019) 294–309, https://doi.org/10.1016/j.actbio.2018.12.017.

[33] H.M. Wong, Y. Zhao, F.K.L. Leung, T. Xi, Z. Zhang, Y. Zheng, S. Wu, K.D.K. Luk, K. M.C. Cheung, P.K. Chu, K.W.K. Yeung, Functionalized polymeric membrane with enhanced mechanical and biological properties to control the degradation of magnesium alloy, Adv. Healthcare Mater. 6 (2017), 1601269, https://doi.org/10.1002/adhm.201601269.

[34] K. Boldbaatar, K. Dashnyam, J.C. Knowles, H.H. Lee, J.H. Lee, H.W. Kim, Dual-ion delivery for synergistic angiogenesis and bactericidal capacity with silica-based microsphere, Acta Biomater. 83 (2019) 322–333, https://doi.org/10.1016/j.actbio.2018.11.025.

[35] Y. Lu, S. Deshmukh, I. Jones, Y.L. Chiu, Biodegradable magnesium alloys for orthopaedic applications, Biomaterials Translational 2 (2021) 214–235, https://doi.org/10.12336/biomatertransl.2021.03.005.

[36] H. Kim, H. Han, K. Lee, D. Lee, J.W. Lee, H. Jeon, S. Cho, H. Roh, Y. Kim, H. Seok, Comprehensive study on the roles of released ions from biodegradable Mg – 5 wt % Ca – 1 wt % Zn alloy in bone regeneration, Journal of Tissu Engineering and Regenerative Medicin 11 (2017) 2710–2724, https://doi.org/10.1002/term.2166.

[37] Y. Yu, G. Jin, Y. Xue, D. Wang, X. Liu, J. Sun, Multifunctions of dual Zn/Mg ion co-implanted titanium on osteogenesis, angiogenesis and bacteria inhibition for dental implants, Acta Biomater. 49 (2017) 590–603, https://doi.org/10.1016/j.actbio.2016.11.067.

[38] S. Bose, G. Fielding, S. Tarafder, A. Bandyopadhyay, W.M. Keck, Understanding of dopant-induced osteogenesis and angiogenesis in calcium phosphate ceramics, Trends Biotechnol. 31 (2013) 594–605, https://doi.org/10.1016/j.tibtech.2013.06.

[39] K. Glenske, P. Donkiewicz, A. Köwitsch, N. Milosevic-Oljaca, P. Rider, S. Rofall, J. Franke, O. Jung, R. Smeets, R. Schnettler, S. Wenisch, M. Barbeck, Applications of metals for bone regeneration, Int. J. Mol. Sci. 19 (2018) 826, https://doi.org/10.3390/ijms19030826.

[40] S. Li, Y. Cui, H. Liu, Y. Tian, G. Wang, Y. Fan, J. Wang, D. Wu, Y. Wang, Application of bioactive metal ions in the treatment of bone defects, J. Mater. Chem. B 10 (2022) 9369–9388, https://doi.org/10.1039/d2tb01684b.

[41] W. Fan, R. Crawford, Y. Xiao, Enhancing in vivo vascularized bone formation by cobalt chloride-treated bone marrow stromal cells in a tissue engineered periosteum model, Biomaterials 31 (2010) 3580–3589, https://doi.org/10.1016/j.biomaterials.2010.01.083.

[42] Z. Huang, Y. Zhang, R. Liu, Y. Li, M. Rafique, A.C. Midgley, Y. Wan, H. Yan, J. Si, T. Wang, C. Chen, P. Wang, M. Shafiq, J. Li, L. Zhao, D. Kong, K. Wang, Cobalt loaded electrospun poly(ε-caprolactone) grafts promote antibacterial activity and vascular regeneration in a diabetic rat model, Biomaterials 291 (2022), https://doi.org/10.1016/j.biomaterials.2022.121901.

[43] C. Wu, Y. Zhou, W. Fan, P. Han, J. Chang, J. Yuen, M. Zhang, Y. Xiao, Hypoxia-mimicking mesoporous bioactive glass scaffolds with controllable cobalt ion release for bone tissue engineering, Biomaterials 33 (2012) 2076–2085, https://doi.org/10.1016/j.biomaterials.2011.11.042.

[44] Z.M. Wright, A.M. Pandit, M.M. Karpinsky, B.D. Holt, E.P. Zovinka, S.A. Sydlik, Bioactive, ion-releasing PMMA bone cement filled with functional graphenic materials, Adv. Healthcare Mater. 10 (2021), https://doi.org/10.1002/adhm.202001189.

[45] Y. Zhuang, A. Liu, S. Jiang, U. Liaqat, K. Lin, W. Sun, C. Yuan, Promoting vascularized bone regeneration via strontium-incorporated hydroxyapatite

bioceramic, Mater. Des. 234 (2023), https://doi.org/10.1016/j.matdes.2023.112313.
[46] J. Duan, Z. Chen, X. Liang, Y. Chen, H. Li, X. Tian, M. Zhang, X. Wang, H. Sun, D. Kong, Y. Li, J. Yang, Construction and application of therapeutic metal-polyphenol capsule for peripheral artery disease, Biomaterials 255 (2020), https://doi.org/10.1016/j.biomaterials.2020.120199.
[47] Y. Kang, C. Xu, L. Meng, X. Dong, M. Qi, D. Jiang, Exosome-functionalized magnesium-organic framework-based scaffolds with osteogenic, angiogenic and anti-inflammatory properties for accelerated bone regeneration, Bioact. Mater. 18 (2022) 26–41, https://doi.org/10.1016/j.bioactmat.2022.02.012.
[48] H. Yang, B. Jia, Z. Zhang, X. Qu, G. Li, W. Lin, D. Zhu, K. Dai, Y. Zheng, Alloying design of biodegradable zinc as promising bone implants for load-bearing applications, Nat. Commun. 11 (2020), https://doi.org/10.1038/s41467-019-14153-7.
[49] M. Chen, Y. Sun, Y. Hou, Z. Luo, M. Li, Y. Wei, M. Chen, L. Tan, K. Cai, Y. Hu, Constructions of ROS-responsive titanium-hydroxyapatite implant for mesenchymal stem cell recruitment in peri-implant space and bone formation in osteoporosis microenvironment, Bioact. Mater. 18 (2022) 56–71, https://doi.org/10.1016/j.bioactmat.2022.02.006.
[50] K. Wang, X. Tong, J. Lin, A. Wei, Y. Li, M. Dargusch, C. Wen, Binary Zn–Ti alloys for orthopedic applications: corrosion and degradation behaviors, friction and wear performance, and cytotoxicity, J. Mater. Sci. Technol. 74 (2021) 216–229, https://doi.org/10.1016/j.jmst.2020.10.031.
[51] Y. Xu, W. Liu, G. Zhang, Z. Li, H. Hu, C. Wang, X. Zeng, S. Zhao, Y. Zhang, T. Ren, Friction stability and cellular behaviors on laser textured Ti–6Al–4V alloy implants with bioinspired micro-overlapping structures, J. Mech. Behav. Biomed. Mater. 109 (2020), https://doi.org/10.1016/j.jmbbm.2020.103823.
[52] D. Pang, Z. Zhang, Y. Zhou, Z. Fu, Q. Li, Y. Zhang, G. Wang, Z. Jing, The process and mechanism for cesium and rubidium extraction with saponified 4-tert-butyl-2-(α-methylbenzyl) phenol, Chin. J. Chem. Eng. 46 (2022) 31–39, https://doi.org/10.1016/j.cjche.2021.07.001.
[53] Z. An, J. Sun, Q. Mei, B. Wei, M. Li, J. Xie, M. He, Q. Wang, Unravelling the effects of complexation of transition metal ions on the hydroxylation of catechol over the whole pH region, J. Environ. Sci. (China) 115 (2022) 392–402, https://doi.org/10.1016/j.jes.2021.08.011.
[54] R.F. Carbonaro, D.M. Di Toro, Linear free energy relationships for metal-ligand complexation: monodentate binding to negatively-charged oxygen donor atoms, Geochem. Cosmochim. Acta 71 (2007) 3958–3968, https://doi.org/10.1016/j.gca.2007.06.005.
[55] L. Feller, Y. Jadwat, R.A.G. Khammissa, R. Meyerov, I. Schechter, J. Lemmer, Cellular responses evoked by different surface characteristics of intraosseous titanium implants, BioMed Res. Int. 2015 (2015), 171945, https://doi.org/10.1155/2015/171945.
[56] J. Zhang, L. Tang, H. Qi, Q. Zhao, Y. Liu, Y. Zhang, Dual function of magnesium in bone biomineralization, Adv. Healthcare Mater. 8 (2019), 1901030, https://doi.org/10.1002/adhm.201901030.
[57] A. Hoppe, N.S. Güldal, A.R. Boccaccini, Biomaterials A review of the biological response to ionic dissolution products from bioactive glasses and glass-ceramics, Biomaterials 32 (2011) 2757–2774, https://doi.org/10.1016/j.biomaterials.2011.01.004.
[58] J. Zhang, L. Tang, H. Qi, Q. Zhao, Y. Liu, Y. Zhang, Dual function of magnesium in bone biomineralization, Adv. Healthcare Mater. 8 (2019), https://doi.org/10.1002/adhm.201901030.
[59] S. Lin, G. Yang, F. Jiang, M. Zhou, S. Yin, Y. Tang, T. Tang, Z. Zhang, W. Zhang, X. Jiang, A magnesium-enriched 3D culture system that mimics the bone development microenvironment for vascularized bone regeneration, Adv. Sci. 6 (2019), https://doi.org/10.1002/advs.201900209.
[60] S. Banai, L. Haggroth, S.E. Epstein, W. Casscells, Influence of Extracellular Magnesium on Capillary Endothelial Cell Proliferation and Migration, n.d. http://ahajournals.org.
[61] Z. Yuan, Z. Wan, C. Gao, Y. Wang, J. Huang, Q. Cai, Controlled magnesium ion delivery system for in situ bone tissue engineering, J. Contr. Release 350 (2022) 360–376, https://doi.org/10.1016/j.jconrel.2022.08.036.
[62] R.M. Visalakshan, A.A. Cavallaro, M.N. MacGregor, E.P. Lawrence, K. Koynov, J. D. Hayball, K. Vasilev, Nanotopography-induced unfolding of fibrinogen modulates leukocyte binding and activation, Adv. Funct. Mater. 29 (2019), https://doi.org/10.1002/adfm.201807453.
[63] W. Qian, L. Gong, X. Cui, Z. Zhang, A. Bajpai, C. Liu, A.B. Castillo, J.C.M. Teo, W. Chen, Nanotopographic regulation of human mesenchymal stem cell osteogenesis, ACS Appl. Mater. Interfaces 9 (2017) 41794–41806, https://doi.org/10.1021/acsami.7b16314.
[64] V. Rodríguez-González, R.B. Domínguez-Espíndola, S. Casas-Flores, O.A. Patrón-Soberano, R. Camposeco-Solis, S.W. Lee, Antifungal nanocomposites inspired by titanate nanotubes for complete inactivation of botrytis cinerea isolated from tomato infection, ACS Appl. Mater. Interfaces 8 (2016) 31625–31637, https://doi.org/10.1021/acsami.6b10060.
[65] P. Gao, B. Fan, X. Yu, W. Liu, J. Wu, L. Shi, D. Yang, L. Tan, P. Wan, Y. Hao, S. Li, W. Hou, K. Yang, X. Li, Z. Guo, Biofunctional magnesium coated Ti6Al4V scaffold enhances osteogenesis and angiogenesis in vitro and in vivo for orthopedic application, Bioact. Mater. 5 (2020) 680–693, https://doi.org/10.1016/j.bioactmat.2020.04.019.
[66] Z. Yuan, Z. Wan, C. Gao, Y. Wang, J. Huang, Q. Cai, Controlled magnesium ion delivery system for in situ bone tissue engineering, J. Contr. Release 350 (2022) 360–376, https://doi.org/10.1016/j.jconrel.2022.08.036.
[67] S. Banai, L. Haggroth, S.E. Epstein, W. Casscells, Influence of Extracellular Magnesium on Capillary Endothelial Cell Proliferation and Migration, n.d. http://ahajournals.org.
[68] C. Wang, B. Zhang, S. Yu, H. Zhang, W. Zhou, R. Luo, Y. Wang, W. Bian, G. Mao, Incorporation of Mg-phenolic networks as a protective coating for magnesium alloy to enhance corrosion resistance and osteogenesis in vivo, J. Magnesium Alloys (2022), https://doi.org/10.1016/j.jma.2022.03.010.
[69] J. Lišková, T.E.L. Douglas, J. Beranová, A. Skwarczyńska, M. Božič, S.K. Samal, Z. Modrzejewska, S. Gorgieva, V. Kokol, L. Bačáková, Chitosan hydrogels enriched with polyphenols: antibacterial activity, cell adhesion and growth and mineralization, Carbohydr. Polym. 129 (2015) 135–142, https://doi.org/10.1016/j.carbpol.2015.04.043.
[70] Y. Gu, J. Zhang, X. Zhang, G. Liang, T. Xu, W. Niu, Three-dimensional printed Mg-doped β-TCP bone tissue engineering scaffolds: effects of magnesium ion concentration on osteogenesis and angiogenesis in vitro, Tissue Eng Regen Med 16 (2019) 415–429, https://doi.org/10.1007/s13770-019-00192-0.
[71] P. Gao, B. Fan, X. Yu, W. Liu, J. Wu, L. Shi, D. Yang, L. Tan, P. Wan, Y. Hao, S. Li, W. Hou, K. Yang, X. Li, Z. Guo, Biofunctional magnesium coated Ti6Al4V scaffold enhances osteogenesis and angiogenesis in vitro and in vivo for orthopedic application, Bioact. Mater. 5 (2020) 680–693, https://doi.org/10.1016/j.bioactmat.2020.04.019.
[72] Q. Li, W. Xiao, F. Zhang, Q. Liu, J. Ye, H. Dong, X. Cao, Tannic acid-derived metal-phenolic networks facilitate PCL nanofiber mesh vascularization by promoting the adhesion and spreading of endothelial cells, J. Mater. Chem. B 6 (2018) 2734–2738, https://doi.org/10.1039/c8tb00350e.
[73] S. Yoshizawa, A. Brown, A. Barchowsky, C. Sfeir, Magnesium ion stimulation of bone marrow stromal cells enhances osteogenic activity, simulating the effect of magnesium alloy degradation, Acta Biomater. 10 (2014) 2834–2842, https://doi.org/10.1016/j.actbio.2014.02.002.
[74] E. Zelzer, W. McLean, Y.-S. Ng, N. Fukai, A.M. Reginato, S. Lovejoy, P.A. D'Amore, B.R. Olsen, Skeletal defects in VEGF120/120 mice reveal multiple roles for VEGF in skeletogenesis, Development 129 (2002) 1893–1904, https://doi.org/10.1242/dev.129.8.1893.